IEEE Transactions on Automation Science and Engineering (T-ASE) paper, presented at ICRA 2026, Vienna, Austria. Cite as T-ASE paper.

Lyapunov Stability-Driven Control Algorithm for Heterogeneous Multi-Robot Coordination

Fatemeh Rekabi-Bana, Mazen Bahaidarah, Ognjen Marjanovic, Farshad Arvin, *Senior Member, IEEE*

***Abstract*—Recent advancements in autonomous swarm systems have made a pivotal point in robotic science. Utilising a large-scale swarm of simple robots to accomplish complex tasks offers efficient, robust, and reliable solutions inspired by natural phenomena. Although bio-inspired methodologies have presented competent algorithms, those approaches inspired by the physical interactions in viscoelastic materials demonstrate more structured methods to prove the stability and robust performance of the algorithms mathematically. This paper proposes a new viscoelastic swarm algorithm which applies to heterogeneous swarm systems. In this paper, the algorithm development utilises the Lyapunov method to determine stability criteria and corresponding conditions. Therefore, the resulting approach does not rely on complex optimisation to obtain the parameters that guarantee stable performance. In addition to the theoretical framework, a series of Monte Carlo simulations have been conducted to assess the algorithm's performance and its sensitivity to the key variables. Furthermore, the algorithm's performance has been evaluated by a series of experiments with real robots to examine the effect of different variables, such as neighbourhood conditions and the stiffness coefficient, on the algorithm's output. The results obtained from the simulations and experiments demonstrate the stable and bounded performance of the algorithm and how the key variables, such as stiffness coefficient and number of neighbours for each robot, affect the swarm performance. The comparison results, obtained from real-world experiments with a state-of-the-art algorithm, show that the proposed framework significantly reduces the control effort for the robots while improving the swarm behaviour.**

***Note to Practitioners:* This paper presents a viscoelastic swarm control algorithm for heterogeneous multi-robot coordination, emphasising stability, robustness, and reduced computational effort. Swarm robotics addresses complex tasks using simple autonomous agents, offering adaptability and resilience. However, practical deployment faces challenges in ensuring system stability and optimising performance under resource constraints. The proposed algorithm applies the Lyapunov method for a theoretical stability proof. Its robustness was validated through Monte Carlo simulations and real-world experiments using the Mona robot platform. Key findings demonstrate that increasing stiffness coefficients enhances swarm cohesiveness but may induce fluctuations in alignment, while a larger number of neighbours and scouts improves alignment stability and robustness. Practitioners in automation, robotics, and related fields can benefit from this work by applying the algorithm to distributed systems requiring efficient coordination under uncertain conditions, such as intelligent transportation and warehouse automation. The approach reduces control effort, a critical factor for battery-operated robots, and offers a systematic framework for parameter tuning based on interaction graph properties. Future work will extend this framework to dynamic interaction networks, extending applicability to real-world scenarios with time-varying constraints.**

***Index Terms*—Heterogenous Swarm, Flocking, Monte Carlo Simulation, Lyapunov method.**

I. Introduction

Swarm control is an innovative solution to large multi-agent robotic system management [1], [2] that is mainly inspired by collective behaviour observed in nature, such as swarms of bees, flocks of birds, and schools of fish [3]. The main purpose of developing control systems to coordinate a large group of autonomous agents is to achieve complex objectives using a group of simple, small robots instead of using a large, complicated system [4]. Following the natural patterns allows the swarm of simple agents to exhibit intricate behaviour, which makes the swarm intelligence a viable candidate for a wide range of applications from autonomous networks [5] to robotic domains due to advantages such as adaptability, scalability, and robustness against uncertainties and failures [6].

Although a wide range of applications can benefit from the capabilities of bio-inspired swarm intelligence [7], [8], developing a practical solution implies resolving challenges such as interaction constraints and unpredictable behaviours [9]. Furthermore, developing a computationally efficient framework is vital, given the limited resources available for each agent's processing unit and the high level of reliability required for many applications, such as intelligent transportation systems [10]. Studying the collaborative behaviour of social animals and insects is the foundation for developing novel swarm intelligence. For instance, [11] investigated the emerging group responses by mimicking the school of fish behaviour, [7] utilised the pheromone communication concept to drive a swarm of robots, and [12] demonstrated different approaches in modelling the bird-flock dynamic to promote the swarm algorithm inspired by nature. Furthermore, other approaches try to use herding behaviours in animals to develop leader-follower structures for swarms of autonomous agents. For instance, [13] made an exclusive review on algorithms inspired by shepherding for swarm control. That work elaborated on the advantages and drawbacks of the shepherding approach that make it complicated for swarm guidance in many practical cases. In another case, the hunting strategy of a grey wolf pack inspired a multi-agent flocking control that benefits from a strict hierarchy

This work was supported by EU H2020-FET-OPEN RoboRoyale project number 964492.

F. Rekabi-Bana and F. Arvin are with the Department of Computer Science, University of Durham, UK. (e-mails: {fatemeh.rekabi-bana, farshad.arvin}@durham.ac.uk)

Mazen Bahaidarah and Ognjen Marjanovic are with the Department of Electrical & Electronic Engineering, University of Manchester, UK.

IEEE Transactions on Automation Science and Engineering (T-ASE) paper, presented at ICRA 2026, Vienna, Austria.

but flexible communication. However, the presented result does not demonstrate scalability for a large number of agents. [14]. However, those investigations mostly focused on describing the collective behaviour when a biological model is applied as an interaction model between robots. Because of the complexities of such models, stability analysis will be difficult or even impossible in particular cases [15].

Other approaches attempt to develop collective motion control methods inspired by the interaction between the particles in elastic materials [16], [17]. Although the simplicity of such frameworks allows for a more convenient implementation and parameter optimisation [18], [19], such algorithms show difficulties regarding marginal stability and fluctuation in some situations [20]. Behavioural swarm is another approach that incorporates more complex methods, such as the fuzzy algorithm, to achieve desirable collective behaviour in complex environments [21]. Other examples of such methods were proposed in [22], applying the hedge algebra to outperform the fuzzy algorithm, and in [23], applying multi-agent reinforcement learning to avoid the requirements for re-training and fine-tuning for each agent individually. Although those methods exhibit reasonable performance in some scenarios, there is no way to analytically investigate the stability and robustness.

Distributed and decentralised control algorithms developed for multi-agent systems allow for the development of frameworks that consider more sophisticated and complex models for the agents and a more intricate communication network [24], [25], [26]. For instance, the development of state and output feedback nonlinear H_∞ algorithms for nonlinear agents proposed in [27] and [28] demonstrated a stable and robust framework for a group of nonlinear agents analytically. Although small-scale multi-agent systems with complex agents can benefit from such algorithms, they would be inefficient for large-scale swarms of simple robots [2].

In this paper, a new self-organised swarm control algorithm is proposed to adopt a viscoelastic interaction between the agents and overcome the marginal stability of the former active elastic sheet (AES) algorithms for swarm control. The development of the new algorithm encompasses a theoretical framework for stability, along with the corresponding conditions for the parameters in this regard. The developed theories not only showcase the asymptotic stability of the coordination algorithm, but also the robustness of the proposed method to bounded perturbations. Previous studies incorporated consensus-based estimation to address the heterogeneous time-varying delays [29], [30] as one of the serious perturbing effects on practical multi-agent systems. However, the proposed framework in this paper applies a different approach to demonstrate the robustness of the coordination to bounded small delays, which is essential for real-world applications. In addition to the theoretical validation, an extensive Monte Carlo simulation was conducted to evaluate the robustness of the algorithm compared to previous forms of AES methods. In the proposed algorithm, the parameters are determined based on the stability criteria and the network configuration of the swarm. Therefore, the computational effort is significantly reduced compared to the cases that require a sophisticated optimisation to calculate the parameters for the algorithm [31], [32]. In addition to the numerical simulation, different series of experiments have been conducted to investigate the performance of the algorithm in different scenarios and how different aspects of the algorithm, such as the neighbourhood condition, the number of different agents, or the stiffness coefficient between the agents, can affect the performance of the algorithm. Therefore, the main contributions of this paper are expressed as follows:

- Development of a distributed and scalable viscoelastic coordination algorithm for heterogeneous multi-agent systems that guarantees a stable tracking of arbitrary time-varying desired formation geometries. The proposed minimal scout-seeker coordination strategy considers a subset of agents (scouts) that are informed about the target geometry, while the remaining agents (seekers) rely solely on local interactions, ensuring distributed coordination with limited global information.
- Systematic method of determining the algorithm's gain based on an analytical approach for asymptotic stability using a structured Lyapunov function and block matrix decomposition that reduces computational burden.
- Robustness analysis of the proposed controller that demonstrates the *Input-to-State Stability (ISS)* in the presence of bounded perturbations and the system's resilience to small communication delays.

Additionally, a sensitivity analysis framework incorporating numerical simulation and experimental setup is introduced to evaluate the algorithm's performance in terms of stability, robustness, and output boundaries.

A. Related Works

Swarm robotics explores different methods of collaboration between the members of a large group of robots. In this domain, early works often featured frameworks inspired by nature, such as foraging [33] and bird flocking [34]. Those bio-inspired algorithms offer decentralised, robust, and scalable control methodologies, particularly for cases where robots have communication and computational capability limitations [35], [36]. However, providing a formal guarantee for stable performance was a challenge, as it is a substantial aspect for practical applications [37].

On the other hand, multi-agent systems (MAS) offered more structured approaches to develop collaborative methods addressing the coordination and communication to obtain collective behaviour [38]. Although MAS approaches demonstrate promising results in cooperative robotic applications such as [39] and benefit from more sophisticated planning and interaction capabilities [40], [41], the computational complexity can be an impediment for practical implementation on large-scale swarms of simple robots [42]. On the other hand, although structured swarm algorithm development frameworks, such as the Fokker-Planck approach [43], offer systematic behavioural predictions, particularly for large-scale statistical key performance indices by considering

IEEE Transactions on Automation Science and Engineering (T-ASE) paper, presented at ICRA 2026, Vienna, Austria.

random elements that affect the agents, they do not address the microscopic stability and coordination of different agents. Accordingly, recent studies aim to apply more structured control theories to enhance the reliability of swarm systems for real-world applications. For instance, incorporating the Lyapunov method yields promising solutions to stability analysis [44], [45], [46].

The viscoelastic model used for robot interaction facilitates the development of a distributed, structured swarm algorithm while maintaining simplicity in the local controllers. That model was inspired by the physical interaction between the particles in elastic materials [47]. Such models are even investigated in different contexts, such as utilising the fluid dynamic model for swarm algorithm development [48]. Furthermore, the research that was outlined in [19] showed the potential of using the viscoelastic model for a heterogeneous swarm of robots.

Addressing the stability criteria mathematically for swarm control algorithms is a complicated procedure [49], [50]. However, applying methods such as Lyapunov theory [51], [52], [53] and eigenvalue analysis [54] enabled the mathematical solution to stability in various cases, including directed and undirected networks, the potential field approach, and interaction based on relative position. Nevertheless, utilising the viscoelastic framework makes the swarm coordination more complicated regarding the analytical stability.

Although the theoretical validation of stability justifies the eligibility of an algorithm, it is necessary to evaluate the algorithm's performance by other approaches, such as numerical simulation and real-world experiments. Monte Carlo simulation is a reliable approach that can handle robustness analysis by considering different types of uncertainties and environmental conditions. Therefore, in multiple studies, that approach was applied to investigate the swarm behaviour in various scenarios [55], [56]. The probabilistic nature of the Monte Carlo simulations allows for studying different aspects of the developed framework, such as potential failure modes, behavioural boundaries, robustness, and the likelihood of achieving the desirable outcome [57]. As a complement to the Monte Carlo simulation for performance evaluation, systematic sensitivity analysis helps determine the significant variables for the algorithm and how the system's outcome varies according to their changes [58]. Therefore, for complex systems such as a swarm of robots, sensitivity analysis provides a valuable perspective on how the algorithm should be implemented to achieve satisfactory results [59].

II. Preliminaries

The following subsections present the preliminary information necessary for algorithm development, specifically regarding the robots' model and graph theory.

A. Robots model

In this paper, each robot is driven by an acceleration command determined according to its interaction with its neighbours and an interactive force with the environment. Therefore, the robots' individual motion can be described as follows:

$$\begin{aligned} \ddot{\mathbf{r}}_i &= \mathbf{F}_i \ , \\ \mathbf{F}_i &= \Sigma_{j\in\mathcal{N}_i}\mathbf{f}_{ij} + \mathbf{f}_i^o \ , \end{aligned} \tag{1}$$

where $\mathbf{r}_i = [x_i, y_i]^T \in \mathbb{R}^2$ is the position vector of the robot i and accordingly the $\ddot{\mathbf{r}}_i \in \mathbb{R}^2$ is the acceleration vector, $\mathbf{F}_i \in \mathbb{R}^2$ is the specific force exerting on the robot i, $\mathbf{f}_{ij} \in \mathbb{R}^2,\ j \in \mathcal{N}_i$ is the contribution of the robot-to-robot interactive force to the specific force regarding the interaction between the robot i and its $j_{th},\ j \in \mathcal{N}_i$ neighbour, $\mathbf{f}_i^o \in \mathbb{R}^2$ represents the contribution to specific force regarding the robot's interaction with the environment and it is determined according to robot's local information.

B. Graph Theory

A swarm of N_{ag} robots that interact with their neighbours can be illustrated by a graph $\mathcal{G}$. Therefore, the graph's node $\nu = \{\nu_i\}_{i=1ag}^{N}$ describes the robots and the edge set $\epsilon \subseteq \nu \times \nu$ describes the interactions between the robots. In this paper, it is assumed that the interactions between the robots are mutual and therefore $\mathbf{f}_{ij} = -\mathbf{f}_{ji}$. Accordingly, the illustrative graph becomes an undirected graph. Furthermore, the neighbourhood for each robot, $\mathcal{N}_i$, can be described as the set of nodes that are connected to the robot's node in the graph by an edge, as presented as follows:

$$\begin{aligned} \epsilon &= \{\epsilon_{ij}\},\ \epsilon_{ij} = (\nu_i, \nu_j) \ , \\ \mathcal{N}_i &= \{\nu_k | \epsilon_{kj} \in \epsilon\} \ . \end{aligned} \tag{2}$$

The adjacency matrix of the graph, $\mathcal{A}_\mathcal{G} \in \mathbb{R}^{N\times N}$, is determined as follows:

$$\begin{aligned} \mathcal{A}_\mathcal{G} &= [a_{ij}], \\ a_{ij} &= \begin{cases} 1 & if \quad (\nu_i, \nu_j) \in \epsilon \\ 0 & otherwise \end{cases} \quad , i, j = 1, ..., N_{ag} \ . \end{aligned} \tag{3}$$

For an undirected graph, the adjacency matrix is symmetric and therefore $a_{ij} = a_{ji}$. Describing the graph degree matrix, $\mathcal{D}_\mathcal{G} \in \mathbb{R}^{N_{ag}\times N_{ag}}$ as a diagonal matrix of each robot's total number of neighbours leads to obtain the Laplacian matrix $\mathcal{L}_\mathcal{G} \in \mathbb{R}^{N_{ag}\times N_{ag}}$ as follows:

$$\mathcal{L}_\mathcal{G} = \mathcal{D}_\mathcal{G} - \mathcal{A}_\mathcal{G} \ . \tag{4}$$

Considering the undirected, time-invariant, and connected structure of the interaction graph, Lemma 1 shows that the Laplacian matrix of the graph presented in (4) is a positive semi-definite matrix [60].

Lemma 1. *if $\{\mathbf{1}\}$ is a column vector with all elements as 1, then 0 is an eigenvalue of the Laplacian matrix $\mathcal{L}_\mathcal{G}$ with $\{\mathbf{1}\}$ as a corresponding right eigenvector and all nonzero eigenvalues have positive real parts. Furthermore, 0 is a simple eigenvalue of $\mathcal{L}_\mathcal{G}$ if and only if there exists a directed spanning tree in $\mathcal{G}$. For an undirected graph $\mathcal{G}$, the smallest nonzero eigenvalue λ_2 of $\mathcal{L}_\mathcal{G}$ satisfies the following*

IEEE Transactions on Automation Science and Engineering (T-ASE) paper, presented at ICRA 2026, Vienna, Austria.

equation [60]:

$$\lambda_2 = \min_{x\neq 0, \{\mathbf{1}\}^T x=0} \frac{x^T \mathcal{L}_{\mathcal{G}} x}{x^T x} \ . \tag{5}$$

III. Collective Motion Control

This section introduces the collective motion behaviour according to the robots' dynamic model discussed in the previous section and the control law proposed in this paper. Afterwards, the Lyapunov approach will be leveraged to demonstrate the controller's effectiveness and validate the stability of the swarm flocking.

A. Flocking Control Policy

The flocking problem in swarm intelligence refers to a situation in which a group of individuals exhibit a dynamic pattern of movement. The flocking pattern, $\mathbb{L} = \{\mathbf{l}_i, \dot{\mathbf{l}}_i, \ddot{\mathbf{l}}_i\}, i = 1, ..., N_{ag}$, the desired flocking pattern is defined by $\mathbf{l}_i \in \mathbb{R}^2$, desired velocity, $\dot{\mathbf{l}}_i \in \mathbb{R}^2$, and desired acceleration vector, $\ddot{\mathbf{l}}_i \in \mathbb{R}^2$, for each robot in the workspace. Therefore, the relative position and velocity between two robots i and j in the desired pattern can be described as $\mathbf{l}_{ij} = \mathbf{l}_j - \mathbf{l}_i$, and $\dot{\mathbf{l}}_{ij} = \dot{\mathbf{l}}_j - \dot{\mathbf{l}}_i$. According to the double integrator model described for the robots in the previous section, the proposed control law for each individual has the structure described in the following equation:

$$\begin{aligned} \mathbf{f}_{ij} &= -\mathbf{k}_{ij}\left(\mathbf{r}_{ij} - \mathbf{l}_{ij}\right) - \mathbf{c}_{ij}\left(\dot{\mathbf{r}}_{ij} - \dot{\mathbf{l}}_{ij}\right) \ , \\ \mathbf{f}_i^o &= -\gamma_i^k(\mathbf{r}_i - \mathbf{l}_i) - \gamma_i^c(\dot{r}_i - \dot{\mathbf{l}}_i) + \ddot{\mathbf{l}}_i \ , \end{aligned} \tag{6}$$

where $\mathbf{r}_{ij} = \mathbf{r}_j - \mathbf{r}_i$ and $\dot{\mathbf{r}}_{ij} = \dot{\mathbf{r}}_j - \dot{\mathbf{r}}_i$ represent the relative position and velocity vector between two robots i and j respectively. Also, $\mathbf{k}_{ij} \in \mathbb{R}^{2\times 2}$ and $\mathbf{c}_{ij} \in \mathbb{R}^{2\times 2}$ demonstrates the stiffness and damping coefficients between two robots i and j respectively. It is assumed that $\mathbf{k}_{ij}$ and $\mathbf{c}_{ij}$ are defined based on the adjacency coefficient between each pair of robots. Furthermore, $\gamma_i^k \geq 0 \in \mathbb{R}^{2\times 2}$ presents the target attraction coefficient for robot i and $\gamma_i^c \geq 0 \in \mathbb{R}^{2\times 2}$ presents the target velocity adjustment coefficient for robot i according to the target point velocity. Also, $\ddot{\mathbf{l}}_i \in \mathbb{R}^2$ represents the target acceleration for robot i. Therefore, each robot is influenced by its neighbour, and meanwhile, it can be affected by the desired position in the target flocking geometry according to (6). Although the proposed controller for each agent considers the position and velocity error, and the target position can have acceleration, it is not necessary to include the acceleration error in the control policy to achieve stability. The following subsection discusses the reason why the proposed control law can stabilise the swarm dynamics following a moving desired geometry, applying the Lyapunov method.

B. Collective Motion Dynamic

In this subsection, the control law introduced in (6) is incorporated to obtain a unified model which describes the entire swarm dynamics. In this study, the interaction network among agents is modelled as a static, undirected, and connected graph, which means that communication links are mutual and do not change over time. According to the robots' model described by (1) and the control policy illustrated by (6), the swarm collective motion dynamics can be described as follows:

$$\begin{bmatrix} \dot{\mathbf{R}} \\ \ddot{\mathbf{R}} \end{bmatrix} = \mathbf{A} \begin{bmatrix} \mathbf{R} \\ \dot{\mathbf{R}} \end{bmatrix} + \mathbf{B}\mathbf{U} \ , \tag{7}$$

where $\mathbf{R} = col\{\mathbf{r}_i\} \in \mathbb{R}^{2N_{ag}}$, $\dot{\mathbf{R}} = col\{\dot{\mathbf{r}}_i\} \in \mathbb{R}^{2N_{ag}}$, $\mathbf{U} = col\{\mathbf{F}_i\} \in \mathbb{R}^{2N_{ag}}$ are the column vector of collective position, velocity, and control vectors respectively. Accordingly, $\mathbf{A} = \begin{bmatrix} [\mathbf{0}]_{2N_{ag}\times 2N_{ag}} & \mathbb{I}_{2N_{ag}} \\ [\mathbf{0}]_{2N_{ag}\times 2N_{ag}} & [\mathbf{0}]_{2N_{ag}\times 2N_{ag}} \end{bmatrix} \in \mathbb{R}^{4N_{ag}\times 4N_{ag}}$ and $\mathbf{B} = \begin{bmatrix} [\mathbf{0}]_{2N_{ag}\times 2N_{ag}} \\ \mathbb{I}_{2N_{ag}} \end{bmatrix}$ are the state and control transition matrices. Considering the joint swarm geometry error as follows:

$$\begin{aligned} \mathbf{E} &= col\{\mathbf{e}_i\}, \ \mathbf{e}_i = \mathbf{r}_i - \mathbf{l}_i, \\ \dot{\mathbf{E}} &= col\{\dot{\mathbf{e}}_i\}, \ \dot{\mathbf{e}}_i = \dot{\mathbf{r}}_i - \dot{\mathbf{l}}_i, \end{aligned} \tag{8}$$

where $\mathbf{E} = \mathbf{R} - \mathbf{L} \in \mathbb{R}^{2N_{ag}}$ and $\dot{\mathbf{E}} = \dot{\mathbf{R}} - \dot{\mathbf{L}} \in \mathbb{R}^{2N_{ag}}$ are the collective vectors represent the flocking error and its time gradient according to the difference between the current swarm collective position vector $\mathbf{R}$ and the desired geometry described by $\mathbf{L} = col\{\mathbf{l}_i\} \in \mathbb{R}^{2N_{ag}}$. According to the control law proposed for each robot in (6), the collective control vector, $\mathbf{U}$, can be described as follows:

$$\mathbf{U} = \begin{bmatrix} -(\mathbf{K}_{\mathcal{G}} + \Gamma) & -\mathbf{C}_{\mathcal{G}} \end{bmatrix} \begin{bmatrix} \mathbf{E} \\ \dot{\mathbf{E}} \end{bmatrix} + \ddot{\mathbf{L}} \ , \tag{9}$$

where $\mathbf{K}_{\mathcal{G}} \in \mathbb{R}^{(2N_{ag}\times 2N_{ag})}$,$\Gamma \in \mathbb{R}^{(2N_{ag}\times 2N_{ag})}$, and $\mathbf{C}_{\mathcal{G}} \in \mathbb{R}^{(2N_{ag}\times 2N_{ag})}$ are defined according to the Laplacian graph $\mathcal{L}_{\mathcal{G}}$ associated with the interaction network between the robots as follows:

$$\begin{aligned} \mathbf{K}_{\mathcal{G}} &= \mathbf{k}_s \otimes \mathcal{L}_{\mathcal{G}} \ , \\ \mathbf{C}_{\mathcal{G}} &= \mathbf{c}_s^{\mathcal{G}} + diag\{\gamma_i^c\} \ , \\ \Gamma &= diag\{\gamma_i^k\} \ , \end{aligned} \tag{10}$$

where $\mathbf{k}_s \in \mathbb{R}^{2\times 2}$ and $\mathbf{c}_s^{\mathcal{G}} \in \mathbb{R}^{2N_{ag}\times 2N_{ag}}$ are the associated swarm stiffness and damping coefficient for each individual according to its interaction with the neighbours, $diag\{.\}$ introduces the operator to make a diagonal matrix from the arguments, and $\otimes$ represents the Kronecker product.

C. Viscoelastic collective control

The swarm coordination algorithm should regulate the integrated state error, which comprises the collective position and velocity errors. Considering the collective motion dynamics introduced by (7), (8), and (9), a collective state error vector can be defined to quantify the weighted flocking geometry tracking error.

$$\mathbf{S} = \begin{bmatrix} \Lambda & [\mathbf{0}]_{2N_{ag}\times 2N_{ag}} \\ [\mathbf{0}]_{2N_{ag}\times 2N_{ag}} & \mathcal{Q} \end{bmatrix} \begin{bmatrix} \mathbf{E} \\ \dot{\mathbf{E}} \end{bmatrix} \ , \tag{11}$$

IEEE Transactions on Automation Science and Engineering (T-ASE) paper, presented at ICRA 2026, Vienna, Austria.

where $\Lambda \in \mathbb{R}^{2N_{ag}\times 2N_{ag}}$ and $\mathcal{Q} \in \mathbb{R}^{2N_{ag}\times 2N_{ag}}$ are positive definite and symmetric weight matrices for collective position and velocity errors. The weighted state error vector enables the controller to adjust the relative importance of position and velocity errors. Therefore, the state error transition for a steady flocking geometry, which implies $\ddot{\mathbf{L}} = 0$, through time can be formulated as follows:

$$\dot{\mathbf{S}} = \begin{bmatrix} [\mathbf{0}]_{2N_{ag}\times 2N_{ag}} & \Lambda \\ -\mathcal{Q}\left(\mathbf{K}_{\mathcal{G}} + \Gamma\right) & -\mathcal{Q}\mathbf{C}_{\mathcal{G}} \end{bmatrix} \begin{bmatrix} \mathbf{E} \\ \dot{\mathbf{E}} \end{bmatrix} . \tag{12}$$

Considering (11) and (12), Theorem 1 demonstrates the conditions that constitute the asymptotic stability for the swarm flocking, which follows an arbitrary time-variant geometry.

Theorem 1. *The collective system described by (12) will be asymptotically stable and converge to the origin, $\mathbf{S} = \mathbf{0}$, if the following conditions are satisfied:*

$$\begin{cases} \mathbf{0} < (\mathbf{K}_{\mathcal{G}} + \Gamma) < \mathbb{I} \\ \mathbf{C}_{\mathcal{G}} = \mathcal{Q}^{-1}\left(\Lambda(\mathbf{K}_{\mathcal{G}} + \Gamma)^{-1}\Lambda + (\mathbf{K}_{\mathcal{G}} + \Gamma)\mathcal{Q}\right) \\ \mathcal{Q} < \Lambda(\mathbf{K}_{\mathcal{G}} + \Gamma)^{-1}\Lambda \\ \mathcal{Q}(\mathbf{K}_{\mathcal{G}} + \Gamma) > \mathbf{0} \end{cases} . \tag{13}$$

Proof. Assuming the Lyapunov function as follows:

$$\begin{aligned} V &= \frac{1}{2}\mathbf{S}^T\mathbf{P}\mathbf{S} , \\ \mathbf{P} &= \begin{bmatrix} (\mathbf{K}_{\mathcal{G}} + \Gamma)^{-1} & \Lambda^{-1} \\ \Lambda^{-1} & \mathcal{Q}^{-1} \end{bmatrix} . \end{aligned} \tag{14}$$

According to the Schur complement theorem and considering the conditions for $\mathcal{Q}$ and Λ in Theorem 1, $\mathbf{P}$ is a symmetric positive definite matrix and therefore the Lyapunov function stated in (14) results in $V > 0 \; if \; \mathbf{S} \neq 0$. Determining the time differentiation of the Lyapunov function results in the following equation:

$$\begin{aligned} \dot{V} &= \mathbf{S}^T\mathbf{P}\dot{\mathbf{S}} \\ &= \begin{bmatrix} \mathbf{E}^T & \dot{\mathbf{E}}^T \end{bmatrix} \begin{bmatrix} \Lambda & \mathbf{0} \\ \mathbf{0} & \mathcal{Q} \end{bmatrix} \mathbf{P} \begin{bmatrix} \mathbf{0} & \Lambda \\ -\mathcal{Q}\left(\mathbf{K}_{\mathcal{G}} + \Gamma\right) & -\mathcal{Q}\mathbf{C}_{\mathcal{G}} \end{bmatrix} \begin{bmatrix} \mathbf{E} \\ \dot{\mathbf{E}} \end{bmatrix}, \end{aligned}$$

considering $\mathbf{P}_t = \begin{bmatrix} \Lambda & \mathbf{0} \\ \mathbf{0} & \mathcal{Q} \end{bmatrix} \mathbf{P} \begin{bmatrix} \mathbf{0} & \Lambda \\ -\mathcal{Q}\left(\mathbf{K}_{\mathcal{G}} + \Gamma\right) & -\mathcal{Q}\mathbf{C}_{\mathcal{G}} \end{bmatrix}$ which is equal to:

$$\mathbf{P}_t = \begin{bmatrix} \Lambda(\mathbf{K}_{\mathcal{G}} + \Gamma)^{-1} & \mathbb{I} \\ \mathcal{Q}\Lambda^{-1} & \mathbb{I} \end{bmatrix} \begin{bmatrix} \mathbf{0} & \Lambda \\ -\mathcal{Q}(\mathbf{K}_{\mathcal{G}} + \Gamma) & -\mathcal{Q}\mathbf{C}_{\mathcal{G}} \end{bmatrix} . \tag{15}$$

By substituting $\mathbf{C}_{\mathcal{G}}$ from (13) and decompose $\mathbf{P}_t$ as a block matrix $\mathbf{P}_t = \begin{bmatrix} \mathbf{P}_t^{11} & \mathbf{P}_t^{12} \\ (\mathbf{P}_t^{12})^T & \mathbf{P}_t^{22} \end{bmatrix}$, the result for each block becomes:

$$\begin{aligned} \mathbf{P}_t^{11} &= -\mathcal{Q}\left(\mathbf{K}_{\mathcal{G}} + \Gamma\right) , \\ \mathbf{P}_t^{12} &= -\left(\mathbf{K}_{\mathcal{G}} + \Gamma\right)\mathcal{Q} , \\ \mathbf{P}_t^{22} &= \mathcal{Q} - \mathcal{Q}\mathbf{C}_{\mathcal{G}} . \end{aligned} \tag{16}$$

According to (16), $\mathbf{P}_t^s = \mathbf{P}_t^{22} - (\mathbf{P}_t^{12})^T(\mathbf{P}_t^{11})^{-1}\mathbf{P}_t^{12}$ can be written as follows:

$$\begin{aligned} &\mathbf{P}_t^s = \mathcal{Q} - \Lambda(\mathbf{K}_{\mathcal{G}} + \Gamma)^{-1}\Lambda - (\mathbf{K}_{\mathcal{G}} + \Gamma)\mathcal{Q} \\ &-(-\mathcal{Q}(\mathbf{K}_{\mathcal{G}} + \Gamma))(-(\mathbf{K}_{\mathcal{G}} + \Gamma)^{-1}\mathcal{Q}^{-1})(-(\mathbf{K}_{\mathcal{G}} + \Gamma)\mathcal{Q}). \end{aligned} \tag{17}$$

Therefore, based on the third condition in (13)

$$\mathbf{P}_t^s = \mathcal{Q} - \Lambda(\mathbf{K}_{\mathcal{G}} + \Gamma)^{-1}\Lambda < \mathbf{0}. \tag{18}$$

Considering the conditions for $\mathcal{Q}$ and $(\mathbf{K}_{\mathcal{G}} + \Gamma)$ in (13), it is evident that $\mathbf{P}_t^{11} < \mathbf{0}$. Consequently, using the Schur complement theory for the block matrices, it is evident that $\mathbf{P}_t < \mathbf{0}$ and therefore:

$$\dot{V} = \begin{bmatrix} \mathbf{E}^T & \dot{\mathbf{E}}^T \end{bmatrix} \mathbf{P}_t \begin{bmatrix} \mathbf{E} \\ \dot{\mathbf{E}} \end{bmatrix} < 0 \; for \; \mathbf{E}, \dot{\mathbf{E}} \neq 0 , \tag{19}$$

which means the system is asymptotically stable. ■

Corollary 1. *The left side of the first condition in (13) will be satisfied if the interaction graph is connected and for at least one robot $\gamma_i^k > \mathbf{0}$.*

Proof. Considering the assumption for mutual interaction with the connected robots and according to Lemma 1, if the interaction graph is connected, then the Laplacian matrix $\mathcal{L}_{\mathcal{G}}$ will be a positive semidefinite with the smallest eigenvalue $\varrho_1 = 0$, and its associated right eigenvector $\vartheta_0 = [\mathbf{1}]_{N_g}$ and the rest of the eigenvalues satisfy $real(\varrho_2, ..., \varrho_{N_{ag}}) > 0$ where ϱ represents the eigenvalue and ϑ represents the right eigenvector of the matrix. Therefore, $\mathbf{K}_{\mathcal{G}}$ inherits the properties of $\mathcal{L}_{\mathcal{G}}$ according to the properties of the Kronecker product and the diagonal structure of $\mathbf{k}_s$ with positive elements. Accordingly, if only one positive definite block exists in Γ, then it satisfies $\Gamma\vartheta_0 \neq 0$ and therefore $\Gamma + \mathbf{K}_{\mathcal{G}}$ becomes positive definite. ■

Corollary 2. *If $\mathbf{k}_s = \begin{bmatrix} k_x & 0 \\ 0 & k_y \end{bmatrix}$, and $k_{max} = max(k_x, k_y)$, then selection of k_{max} as $k_{max} < \frac{1-\gamma_{max}}{2d_{max}}$, where d_{max} is the maximum degree in the interaction graph and $\gamma_{max} = max(\gamma_i^k)$, satisfies the right hand side of the first inequality in (13).*

Proof. According to the properties of the Kronecker product, the maximum eigenvalue of $\mathbf{K}_{\mathcal{G}}$ can be determined as

$$\varrho_{max}(\mathbf{K}_{\mathcal{G}}) = k_{max}\varrho(\mathcal{L}_{\mathcal{G}}) .$$

On the other hand, according to Weyl's inequality theorem for the eigenvalues, the upper bound of the spectrum for $\varrho(\mathbf{K}_{\mathcal{G}} + \Gamma)$ is $\varrho(\mathbf{K}_{\mathcal{G}}) + \gamma_{max}$. Considering the upper bound of the spectrum for the Laplacian matrix as $\varrho(\mathcal{L}_{\mathcal{G}}) \leq 2d_{max}$, it concludes:

$$\varrho(\mathbf{K}_{\mathcal{G}} + \Gamma) \leq \varrho(\mathbf{K}_{\mathcal{G}}) + \gamma_{max} \leq 2k_{max}d_{max} + \gamma_{max} .$$

Therefore, if $k_{max} < \frac{1-\gamma_{max}}{2d_{max}}$ then

$$\varrho(\mathbf{K}_{\mathcal{G}} + \Gamma) < 1 .$$

According to the Hermitian structure of the $\mathbf{K}_{\mathcal{G}} + \Gamma$, the singular values and the eigenvalues are equivalent, and therefore $(\mathbf{K}_{\mathcal{G}} + \Gamma) < \mathbb{I}$. ■

Corollary 3. *Considering $\rho(\mathcal{Q}) < \frac{\varrho_{min}(\Lambda)^2}{2k_{max}d_{max}+\gamma_{max}}$, where $\rho(.) = \sup(\varrho(.))$ represents the spectral radius of its argument, then the third condition of (13) will be constituted.*

IEEE Transactions on Automation Science and Engineering (T-ASE) paper, presented at ICRA 2026, Vienna, Austria.

Proof. The stated condition in this corollary implies:

$$\frac{\varrho_{min}(\Lambda)^2}{\rho(\mathcal{Q})} > 2k_{max}d_{max} + \gamma_{max} \geq \rho(\mathbf{K}_\mathcal{G} + \Gamma). \quad (20)$$

On the other hand, because $\mathcal{Q}$ and Λ are positive definite and symmetric matrices, according to the Rayleigh quotient:

$$\frac{\mathbf{x}^T(\Lambda\mathcal{Q}^{-1}\Lambda)\mathbf{x}}{\mathbf{x}^T\mathbf{x}} = \frac{(\Lambda\mathbf{x})^T\mathcal{Q}^{-1}(\Lambda\mathbf{x})}{\mathbf{x}^T\mathbf{x}}, \quad (21)$$

is valid for any arbitrary vector $\mathbf{x}$. Furthermore, $(\Lambda\mathbf{x})^T\mathcal{Q}^{-1}(\Lambda\mathbf{x}) \geq \frac{1}{\rho(\mathcal{Q})}(\Lambda\mathbf{x})^T(\Lambda\mathbf{x})$. Therefore,

$$\frac{\mathbf{x}^T(\Lambda\mathcal{Q}^{-1}\Lambda)\mathbf{x}}{\mathbf{x}^T\mathbf{x}} \geq \frac{1}{\rho(\mathcal{Q})}\frac{\mathbf{x}^T\Lambda^2\mathbf{x}}{\mathbf{x}^T\mathbf{x}} \geq \frac{\varrho_{min}(\Lambda^2)}{\rho(\mathcal{Q})}. \quad (22)$$

Accordingly,

$$\frac{\mathbf{x}^T(\mathbf{K}_\mathcal{G} + \mathbf{\Gamma})\mathbf{x}}{\mathbf{x}^T\mathbf{x}} \leq \rho(\mathbf{K}_\mathcal{G} + \mathbf{\Gamma}) < \frac{\varrho_{min}(\Lambda^2)}{\rho(\mathcal{Q})}. \quad (23)$$

Therefore, $\frac{\mathbf{x}^T(\mathbf{K}_\mathcal{G}+\mathbf{\Gamma})\mathbf{x}}{\mathbf{x}^T\mathbf{x}} < \frac{\mathbf{x}^T(\Lambda\mathcal{Q}^{-1}\Lambda)\mathbf{x}}{\mathbf{x}^T\mathbf{x}}$ which means $(\mathbf{K}_\mathcal{G} + \mathbf{\Gamma}) < \Lambda\mathcal{Q}^{-1}\Lambda$ and it is equivalent to $\mathcal{Q} < \Lambda(\mathbf{K}_\mathcal{G} + \mathbf{\Gamma})^{-1}\Lambda$ that constitutes the third condition in (13). ■

Corollary 4. *The perturbed collective system described by:*

$$\dot{\mathbf{S}} = \begin{bmatrix} [\mathbf{0}]_{2N_{ag}\times 2N_{ag}} & \Lambda \\ -\mathcal{Q}\left(\mathbf{K}_\mathcal{G} + \Gamma\right) & -\mathcal{Q}\mathbf{C}_\mathcal{G} \end{bmatrix} \begin{bmatrix} \mathbf{E} \\ \dot{\mathbf{E}} \end{bmatrix} + \Delta_\mathcal{E}\ , \quad (24)$$

where $\Delta_\mathcal{E} \in \mathbb{R}^{4N_{ag}}$ is the bounded perturbations on collective state, is Input-to-State Stable (ISS) with the Lyapunov gain function:

$$\mathcal{X}(r) = \frac{1}{(1-\varepsilon)\sigma_{max}(\mathcal{A}_s)}r, \quad (25)$$

where $0 < \varepsilon < 1$ is a small gain and r is a positive scalar value and $\mathcal{A}_s = \begin{bmatrix} [\mathbf{0}]_{2N_{ag}\times 2N_{ag}} & \Lambda \\ -\mathcal{Q}\left(\mathbf{K}_\mathcal{G} + \Gamma\right) & -\mathcal{Q}\mathbf{C}_\mathcal{G} \end{bmatrix}$.

Proof. Considering the Lyapunov function introduced in (14) for the perturbed system in (24) results in the following equation for the time derivative of the Lyapunov function:

$$\dot{V} = \mathcal{E}^T\mathbf{P}_t\mathcal{E} + \mathcal{E}^T\begin{bmatrix} \Lambda & \mathbf{0} \\ \mathbf{0} & \mathcal{Q} \end{bmatrix}\mathbf{P}\Delta_\mathcal{E}, \quad (26)$$

where $\mathcal{E} = \begin{bmatrix} \mathbf{E} \\ \dot{\mathbf{E}} \end{bmatrix}$. Assuming $|\mathcal{E}| > \mathcal{X}(|\Delta_\mathcal{E}|)$, where $|.|$ returns the second norm of its argument, with the Lyapunov gain stated in (25) concludes:

$$\dot{V} \leq -\sigma_{max}(\mathbf{P_t})|\mathcal{E}|^2 + (1-\varepsilon)\sigma_{max}(\mathbf{P_t})|\mathcal{E}|^2, \quad (27)$$

where $\sigma_{max}(\mathbf{P_t})$ is the maximum singular value associated with $\mathbf{P}_t$. Therefore, $\dot{V} \leq -\varepsilon\sigma_{max}(\mathbf{P_t})|\mathcal{E}|^2, \forall\mathcal{E} \neq 0$ which means that the perturbed system in (24) is ISS according to the Lyapunov gain described in (25) according to [61]. ■

Corollary 4 shows that the proposed coordination algorithm is robust against bounded small perturbations from the environment and internal uncertainties. Therefore, although the algorithm does not directly encounter stochasticity over the communication network, the ISS feature of the algorithm demonstrates its robustness against bounded perturbations, which can include uncertainties modelled as bounded stochastic processes. Therefore, if random disturbances or bounded uncertainties affect individual agents, as often considered in stochastic consensus [62], [63], the system's collective stability remains preserved. Time delay is one of the sources that causes perturbations in the collective motion. As stated in (6), the interaction between the agents depends on the calculation of relative position and velocity. However, considering the time delay in receiving the data implies:

$$\tilde{\mathbf{f}}_{ij} = -\mathbf{k}_{ij}\left(\tilde{\mathbf{r}}_{ij} - \mathbf{l}_{ij}\right) - \mathbf{c}_{ij}\left(\tilde{\dot{r}}_{ij} - \dot{\mathbf{l}}_{ij}\right)\ , \quad (28)$$

where $\tilde{\mathbf{r}}_{ij} = \mathbf{r}_j(t-\tau) - \mathbf{r}_i(t)$ and $\tilde{\dot{\mathbf{r}}}_{ij} = \dot{\mathbf{r}}_j(t-\tau) - \dot{\mathbf{r}}_i(t)$ are the relative position and velocity associated with the communication delay τ between agents i and j. The following theorem shows that the proposed coordination system is robust against small communication delays according to the ISS feature demonstrated in Corollary 4.

Theorem 2. *The collective system associated with the communication delay and the agent-to-agent interactions described in (28) is stable if $\mathbf{r}_k(t)$ and $\dot{\mathbf{r}}_k(t)$ are Lipschitz for all agent k.*

Proof. Considering the coordination law in (28), the collective state error dynamic becomes:

$$\dot{\mathbf{S}} = \mathcal{A}_s\begin{bmatrix} \mathbf{E} \\ \dot{\mathbf{E}} \end{bmatrix} + \begin{bmatrix} \mathbf{0} \\ \Delta_\mathbf{U} \end{bmatrix}, \quad (29)$$

where $\Delta_\mathbf{U} = \{\Delta u_i\}$ and

$$\Delta u_i = \Sigma_{j\in\mathcal{N}_i}\left(-k_{ij}\delta\mathbf{r}_j(\tau_{ij}) - c_{ij}\delta\dot{\mathbf{r}}_j(\tau_{ij})\right),$$

where $\delta\mathbf{r}_j(\tau_{ij}) = \mathbf{r}_j(t) - \mathbf{r}_j(t-\tau_{ij})$ and $\delta\dot{\mathbf{r}}_j(\tau_{ij}) = \dot{\mathbf{r}}_j(t) - \dot{\mathbf{r}}_j(t-\tau_{ij})$. If $\mathbf{r}_k$ and $\dot{\mathbf{r}}_k$ are Lipschitz functions, then:

$$\begin{aligned} |\delta\mathbf{r}_j(\tau_{ij})| &= |\mathbf{r}_k(t-\tau) - \mathbf{r}_k(t)| \leq L_r\tau_{ij} \\ |\delta\dot{\mathbf{r}}_j(\tau_{ij})| &= |\dot{\mathbf{r}}_k(t-\tau) - \dot{\mathbf{r}}_k(t)| \leq L_{\dot{r}}\tau_{ij}. \end{aligned} \quad (30)$$

Therefore, $|\Delta u_i| \leq d_i(k_{max}L_r + c_{max}L_{\dot{r}})\tau_{max}$ where τ_{max} is the maximum experienced delay in communication and $c_{max} = \max\{c_{ij}\}$. Accordingly, $|\Delta_\mathbf{U}| \leq \kappa\tau_{max}$ where κ is a positive constant. Therefore, the collaborative system associated with the communication delay can be considered as a perturbed system with the bounded perturbation $\begin{bmatrix} \mathbf{0} & \Delta_\mathbf{U}^T \end{bmatrix}^T$. Subsequently, the perturbed system described in (29) remains stable for small time delays because of the ISS feature according to Corollary (4). ■

In this paper, two types of robots are considered for the simulations and experiments. The first type is associated with robots that have information about their own target destination and an attraction force in that direction. In this paper, these robots are referred to as scouts. The second type is associated with those robots that do not have direct information about their destination or target points, and they should reach the target by merely implementing the first part of the interaction law with their neighbours according to (6).

IEEE Transactions on Automation Science and Engineering (T-ASE) paper, presented at ICRA 2026, Vienna, Austria.

In this paper, the second type of robot is referred to as a seeker. According to the theoretical analysis presented above, a heterogeneous swarm system can achieve a target formation geometry with both types of robots present in the swarm. It is evident that the proposed framework is different from general leader-follower algorithms because:

- The seeker robots do not necessarily have direct interactions with the scouts.
- The scout's behaviour is not independent of the seeker robots, as they have mutual interaction. In fact, despite the additional local controller that scouts apply to follow their target, they have the same interaction as seekers with their neighbours.
- The scouts can be neighbours and interact with each other.

Each agent can interact with zero, one, or more than one scout. Also, scouts can interact and be neighbours with each other. In this study, being a scout does not contribute directly to agent-to-agent interaction law. However, those scouts use the target information, incorporating the local control law stated as $\mathbf{f}_i^o$ in (6) to follow the targets and, accordingly, affect the entire swarm. Corollary 1 shows that if only one scout exists in the swarm, then the stability criteria can be determined, and the swarm can reach the target points. Furthermore, Corollary 2 offers an upper bound for the stiffness coefficient to guarantee the second stability criterion in (13). Considering all the conditions stated in (13) and Corollaries (1) to (3) allows a straightforward process to find the parameters for stiffness and damping coefficients according to the structure of the interaction graph $\mathcal{G}$.

The implementation of the proposed control law involves relative position and velocity measurements with local neighbours, resulting in computational complexity of $\mathcal{O}(d_i)$, where d_i is the number of neighbours for agent i. The weighting matrices Λ, $\mathcal{Q}$, and Γ are diagonal and require negligible computation. However, the damping matrix $\mathbf{C}_\mathcal{G}$ is not diagonal and depends on the global structure presented in 13. As $\mathbf{K}_\mathcal{G} + \Gamma$ is symmetric and typically sparse due to its Laplacian structure, efficient numerical methods such as sparse Cholesky factorization can be applied to compute or approximate $(\mathbf{C}_\mathcal{G})$ in $\mathcal{O}(N_{ag}^2)$ [64]. Therefore, the framework maintains a balance between formal stability guarantees and computational feasibility in swarm-scale implementations. In the next section, a series of numerical simulations is presented to assess the effectiveness of the proposed swarm control framework, along with a sensitivity analysis of the key variables in the algorithm.

IV. Numerical Simulation Results

This section presents the structure of the numerical simulations and the results obtained for evaluating the performance of the proposed algorithm. The Monte Carlo method is utilised for statistical analysis of the system's output in different situations. The network graph between the agents is determined according to two assumptions.

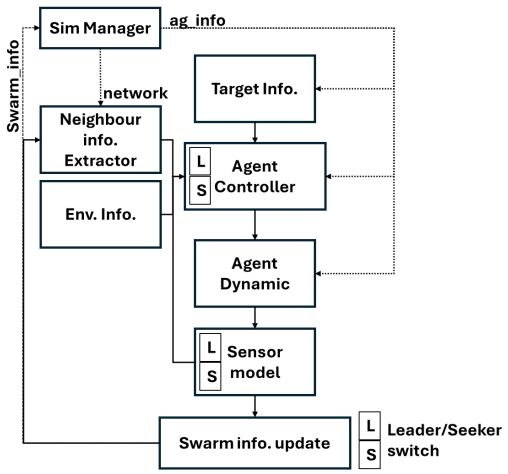

Figure 1. Simulation process for the swarm behaviour considering the implemented algorithm.

- The first assumption is associated with the number of neighbours and the eligible distance for the neighbourhood in the target swarm geometry.
- The second assumption is to establish an undirected and connected graph between the agents.

Therefore, each agent has at least N_{Neb} neighbours, and if agent j is one of the neighbours for agent i, then agent i is also a neighbour for agent j. According to the theoretical development, the network graph between the agents should be connected, but it does not need to be fully connected. In each simulation, the robots are placed as a square shape in a two-dimensional arena with a size $L \times L$, each of which is assigned a random angle $\theta \in [0, 2\pi]$. The desired geometry when the swarm reach the destination location is a hexagonal shape. The main parameters that are used in the simulations are listed in I. In this study, two types of robots are considered. The first type is the scout associated with those robots that have information about the target points, and the second type is the seeker that may or may not have direct interaction with the scouts. In the Monte-Carlo simulations, the scouts were selected randomly to assess different conditions. Therefore, each agent may interact with none, one, or more than one scout. The flowchart in Fig. 1 schematically demonstrates the simulation process. As demonstrated in Fig. 1, the developed simulation environment comprises general modules for the robots' dynamic model, controller implementation, sensor model, and data extractor. The robot controller and sensor module have different structures for different types of robots. The controller module implements the local control policy stated in (6) according to the feedback from the sensor module and other information, depending on the robot's type.

To create a more realistic simulation, the sensor module adds measurement noise to the position vector, which is updated by the robot's model module. The measurement noise also acts as a bounded disturbance on the system. Therefore, the coordination system should regulate the effect of that disturbance to stabilise the system. This is the

IEEE Transactions on Automation Science and Engineering (T-ASE) paper, presented at ICRA 2026, Vienna, Austria.

Table I
MAIN PARAMETERS USED FOR THE NUMERICAL SIMULATIONS.

Parameters	Description	Values
N_{ag}	Swarm size	100 robots
N_L	Number of scouts	{1,4,8,15}
N_{Neb}	Number of Neighbours	{2,4,6,10}
k	Spring constant	{0.02,0.05,0.1,0.15}
γ	Attraction coefficient	0.2
L	Arena's side length	100 m
R_s	Sensing radius	2 m
T_{sim}	Simulation time	950 s
η	Measurement noise	$\mathcal{U}(-0.01, 0.01)$

key element for showcasing the robustness of the proposed algorithm and evaluating the boundedness of the output in various situations. The final part of the simulation setup is the simulation manager, which is responsible for distributing the latest information about the robots to the entire swarm and the interaction network between them. The parameters applied to the simulation and the coordination algorithm are listed in Table I.

The Monte Carlo method was implemented by conducting 50 simulations to evaluate collective motion performance. Based on the described simulation environment, three distinct cases are designed to study the impact of (i) neighbour links, (ii) multiple scouts, and (iii) variation of spring coefficient value. In each case, the total force (F_T), the alignment (ψ), and the cohesiveness (D) are the performance metrics used to examine the robustness and stability of each case. The total force F_T is a significant indicator of the interaction forces within the swarm that measures how the robots deviate from their desired relative positions. F_T can be expressed as the summation of all interaction forces for the swarm of size N:

$$F_T = \sum_{i=1}^{N_{ag}} \|\mathbf{F}_i\| \ , \tag{31}$$

where $\mathbf{F}_i$ denotes the exerted force on the robot i, as defined in (1). A high value of the total force indicates significant positional differences between robots, which may not have reached their equilibrium positions. As the robots decrease their positional errors over time, the total force decreases. The degree of alignment is another key metric to demonstrate the alignment status of the swarm denoted as ψ in (32). In a case where all robots are aligned in a consensus direction, $\psi \approx 1$. Conversely, a disordered swarm, characterised by random orientations among robots, results in $\psi \approx 0$. The degree of alignment ψ can be described as follows:

$$\psi = \frac{1}{N_{ag}} \left\| \sum_{i=1}^{N_{ag}} \hat{\mathbf{n}}_i \right\| , \hat{\mathbf{n}}_i = \begin{bmatrix} \cos(\theta_i) \\ \sin(\theta_i) \end{bmatrix}, \tag{32}$$

where θ_i represents the direction of motion for robot i, and $\hat{n}_i$ is a unit vector that is aligned with the robot's direction. In addition, the swarm's cohesiveness D is a metric that quantifies the consistency in the spatial structure of the swarm [19]. Specifically, evaluating how well the robots maintain their positions relative to the swarm's centre of mass. D can be calculated based on the distances between each robot and the swarm's centre:

$$\mu_c = \frac{\sum_{i=1}^{N_{ag}} \|\mathbf{r}_i - \mathbf{r}_c\|}{N_{ag}}, \sigma_c = \sqrt{\frac{\sum_{i=1}^{N_{ag}} (\|\mathbf{r}_i - \mathbf{r}_c\| - \mu_c)^2}{N_{ag} - 1}},$$
$$D = \frac{\sigma_c}{\mu_c} \ . \tag{33}$$

In (33), r_i is the relative position of the robot i, and r_c denotes the centre of mass of the swarm. μ_c is the average distance of the robots from the centre of mass, and σ_c is the standard deviation of these distances. For the swarm to maintain a stable structure, D must remain relatively consistent throughout the simulation.

In each case, the measurement noise on the agents' position vector introduces a disturbance to coordination, and the algorithm must regulate the effect of this disturbance to stabilise the swarm and ensure boundedness of the output.

A. Case 1: Different Neighbour Links

For this analysis, a swarm of $N = 100$ robots are placed in the arena in a square shape, and their destination shape is determined as a pentagon. The swarm will have only one scout, and the rest of the parameters will be fixed, as shown in Table I. The following set for the number of neighbour links $N_{Neb} \in \{2, 4, 6, 10\}$ is considered. For each case, 50 simulations have been conducted with different sets of initial conditions for position, velocity, and angles. The interaction network for each simulation was determined according to the final formation configuration. The results obtained from each set of simulations are shown in Fig. 2.

According to the results for the alignment, Fig. 2 shows that the fluctuation in the contours diminishes when the number of neighbours increases. It is clear that increasing the number of links between the robots enables them to reach full alignment more quickly. Furthermore, alignment variation reduces significantly in the transient region, which helps the robots move together more consistently. However, relying on a high number of interaction links is not practical in real-world applications. Therefore, such a sensitivity analysis helps to find the admissible performance region. On the other hand, the probability distribution of the cohesiveness shows that the cohesiveness values move to the lower values as the number of links increases. Therefore, the swarm structure becomes more solid by increasing the number of links.

B. Case 2: Different Number of Scouts

In the second sensitivity analysis, the number of scouts is considered a key variable that can affect the swarm's performance. Scouts are robots that exhibit similar dynamics and interaction models with their neighbours, while possessing information about the target position and being able to measure the distance to their destination point. Therefore, increasing or decreasing the number of those robots can affect the entire swarm's performance. To assess the effect of the number of scouts, a swarm of $N = 100$ robots is placed in the arena in a square shape, and their destination shape is determined

IEEE Transactions on Automation Science and Engineering (T-ASE) paper, presented at ICRA 2026, Vienna, Austria.

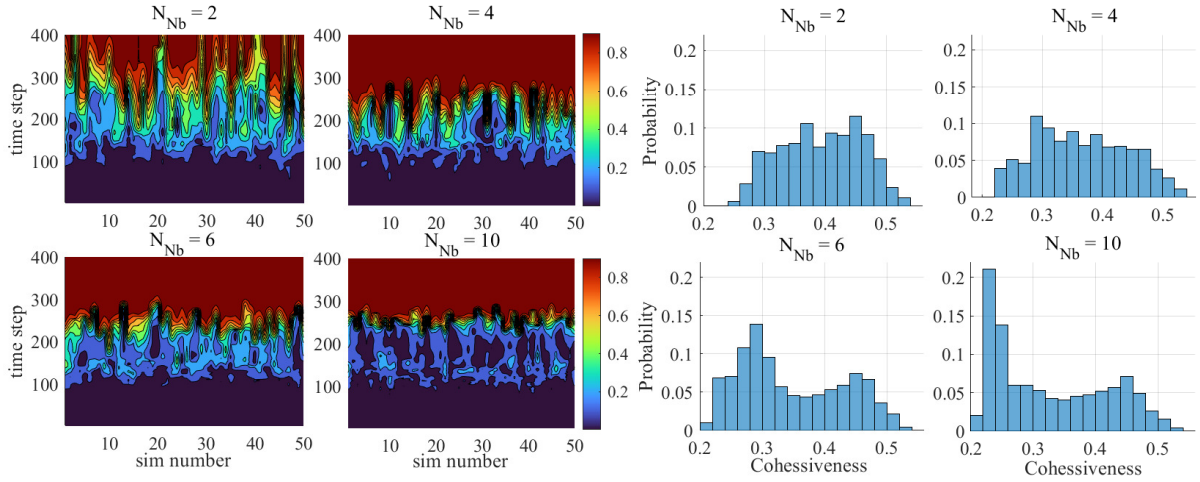

Figure 2. The sensitivity analysis for the number of neighbours. (left)-The contour variation of the alignment according to the Monte Carlo simulation. (right)-The probability distribution of the cohesiveness according to the Monte Carlo simulation.

as a pentagon. Each robot in the swarm will be connected to four neighbouring links. The following set for the number of scouts $N_L \in \{1, 4, 8, 15\}$ is considered for sensitivity analysis. The rest of the parameters will be fixed, as shown in Table I. For each case, a set of 50 simulations is conducted, with random robots as the scouts. The initial conditions and the interaction network are set in the same way as described in the previous case. The statistical results obtained from those sets of simulations are presented in Fig. 3. According to the contour plot of the alignment obtained from the Monte Carlo analysis in Fig. 3, increasing the number of scouts reduces the fluctuation in alignment significantly, particularly in the transient region. However, changing the number of scouts from 8 to 15 does not show substantial variations in the alignment contours. Therefore, it is evident that the improvement of the alignment index reaches an upper bound. On the other hand, increasing the number of scouts shifts the cohesiveness values from lower to higher values, resulting in more pronounced geometrical fluctuations in the swarm formation. According to the presented sensitivity analysis, it is evident that the selection of the number of scouts depends on the importance and priority of the alignment, as well as the cohesiveness of the swarm.

C. Case 3: Different stiffness Coefficients

The third key variable in the proposed algorithm is the stiffness coefficient applied in the local control policy. According to the results obtained in the mathematical development, the stiffness coefficient is a determinant factor in the swarm's stability. Therefore, it is necessary to evaluate the sensitivity of the algorithm's performance to the variation of this parameter. It allows for the selection of the best stiffness range according to the swarm structure. Consequently, a swarm of $N = 100$ robots are considered in the same way as the previous analysis and the values for the stiffness coefficient values are selected from the set: $k \in \{0.02, 0.05, 0.1, 0.15\}$. The swarm structure remains constant through this analysis, and the initial conditions are set in the same way as in previous studies. The results obtained from four sets of Monte Carlo simulations are demonstrated in Fig. 4.

As presented in the contour graph in Fig. 4, the alignment fluctuation increases significantly when the stiffness coefficient increases. On the other hand, cohesiveness is pushed to lower values, which increases the rigidity of the formation geometry. Considering a fixed swarm structure (with a similar interaction network and a number of scouts), increasing the stiffness forces the swarm to maintain a more solid structure, as indicated by the cohesiveness results. However, the effect of the stiffness coefficient on the geometrical rigidity is different from the way that the number of neighbours can affect the swarm's solidity. Increasing the number of neighbours causes a more stable resultant force on each robot, although fewer but stronger links can lead to vibrational behaviour for the robot. Therefore, despite the significant improvement in cohesiveness, increasing the stiffness coefficient increases the energy lost, which is a drawback, particularly for small robots that have limited power sources.

In addition to the sensitivity analysis regarding the alignment and cohesiveness indices, a quantitative result is presented in Table II to compare the statistical indices, minimum (min), maximum (max), median, and interquartile range (IQR) for the total force of the swarm as a representative of the control effort that the algorithm imposes on the swarm to reach the target formation.

According to the results demonstrated in Table II, it is evident that the control effort is linearly sensitive to the stiffness coefficient and the number of neighbours according to the median index, although it is not significantly sensitive to the number of scouts. Furthermore, the statistical results showcase the boundedness of the system's output in all cases, while the measurement noise acts as a disturbing effect on the algorithm's performance. Therefore, the numerical simulation validates the robustness feature of the algorithm in the presence of bounded disturbances.

IEEE Transactions on Automation Science and Engineering (T-ASE) paper, presented at ICRA 2026, Vienna, Austria.

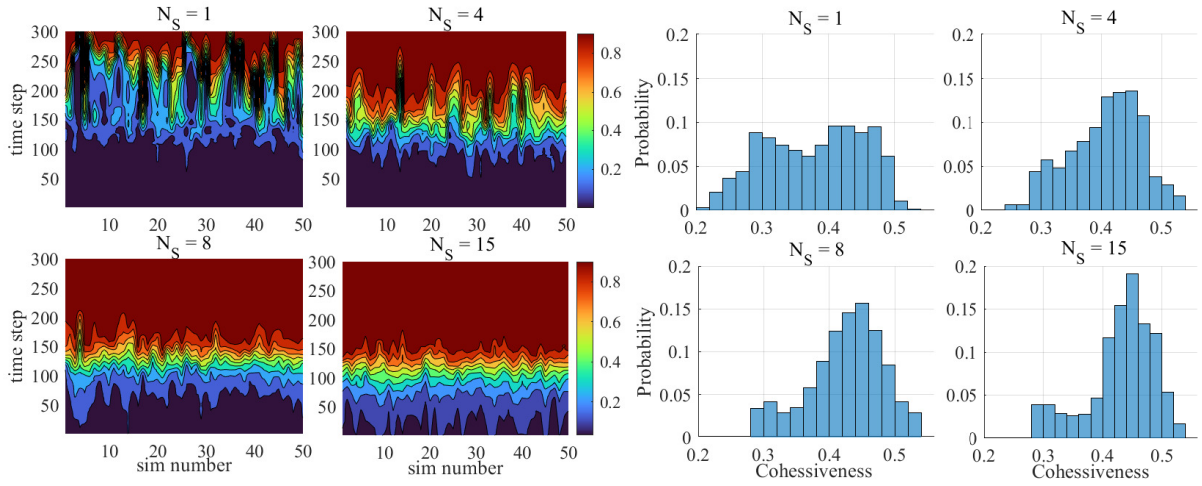

Figure 3. The sensitivity analysis for the number of scouts. (left)-The contour variation of the alignment according to the Monte Carlo simulation. (right)-The probability distribution of the cohesiveness according to the Monte Carl simulation.

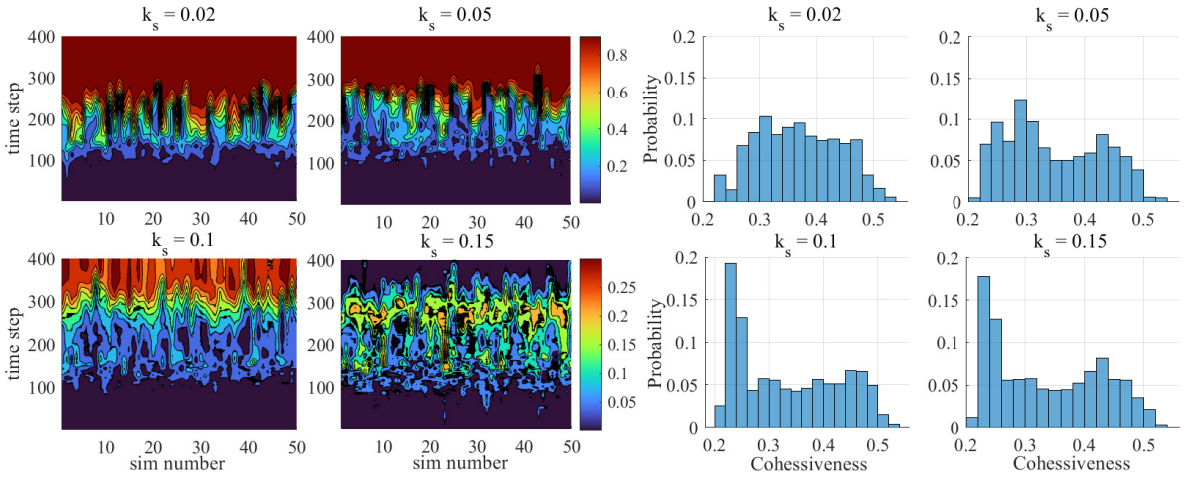

Figure 4. The sensitivity analysis for the stiffness coefficient. (left)-The contour variation of the alignment according to the Monte Carlo simulation. (right)-The probability distribution of the cohesiveness according to the Monte Carlo simulation.

Table II
STATISTICAL ANALYSIS OF THE TOTAL FORCE IN THE FIRST 200 TIME STEPS IN THREE SENSITIVITY ANALYSIS CASES

Simulation Case		min	max	median	IQR
Base Case $k = 0.02; N_{Neb} = 4; N_L = 1$		1.034	82.15	12.19	38.36
Sensitivity to stiffness $N_{Neb} = 4; N_L = 1$	$k = 0.05$	1.86	177.66	30.84	89.87
	$k = 0.1$	7.3	354.15	64.59	181.28
	$k = 0.15$	11.87	533.16	99.04	273.3
Sensitivity to N_{Neb} $k = 0.02; N_L = 1$	$N_{Neb} = 2$	0.57	42.19	4.95	16.92
	$N_{Neb} = 6$	1.34	104.94	16.94	50.45
	$N_{Neb} = 10$	2.82	166.47	31.83	84.7
Sensitivity to N_L $k = 0.02; N_{Neb} = 4$	$N_L = 4$	2.168	71.51	10.99	31.57
	$N_L = 8$	4.08	73.42	12.75	31.34
	$N_L = 15$	7.39	74.63	15.49	29.34

V. EXPERIMENT RESULT

A. Swarm Robotics Platform

The Mona open-source miniature robot, illustrated in Fig. 5, was developed for applications in swarm robotics [65]. This cost-effective and user-friendly mobile robot is suitable for both educational and research purposes. Mona is equipped with an ESP32-WROVER-B System-on-a-Chip (SoC), which operates at a frequency of up to 240 MHz and includes 4 MB of flash memory along with 8 MB of SRAM. The robot's mobility is driven by two DC motors, enabling it to achieve a maximum speed of 10 $\mathrm{cm/s}$. Five evenly distributed infrared (IR) sensors are installed on the robot's front side to facilitate proximity sensing. Additionally, Mona is equipped with a Wi-Fi module that enables wireless communication, promoting interaction with other robots within the swarm. Although the robots are similar, the physical parameters, such as actuation uncertainty, communication delays, and measurement noise, add disturbances to the coordination framework. Therefore, the results of these experiments not only showcase the practical capability of the algorithm but also validate its robustness against such bounded disturbances and uncertainties as shown theoretically in Section III.

IEEE Transactions on Automation Science and Engineering (T-ASE) paper, presented at ICRA 2026, Vienna, Austria.

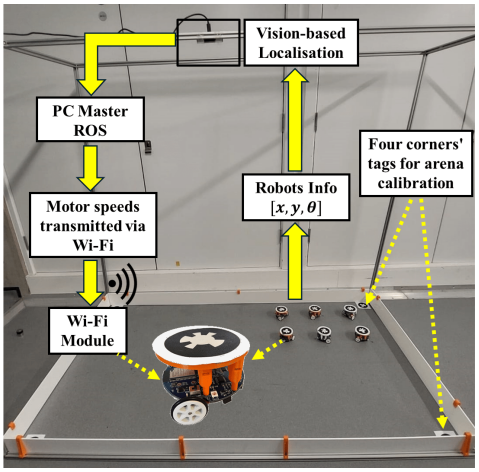

Figure 5. The robot arena used for the experiments, including a vision system for localisation and a ROS network for communication between the nodes

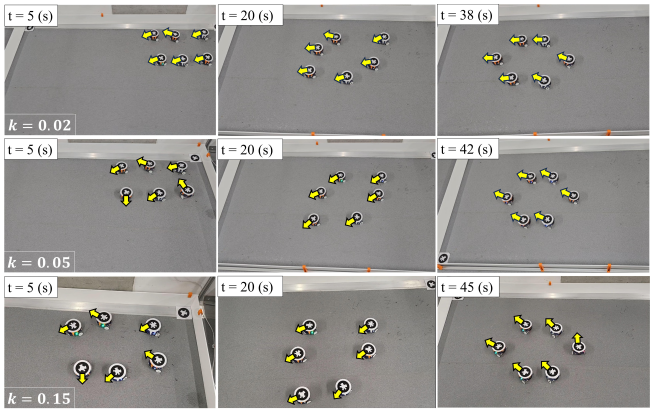

Figure 6. The video frames from the experiments on sensitivity analysis for the stiffness coefficient

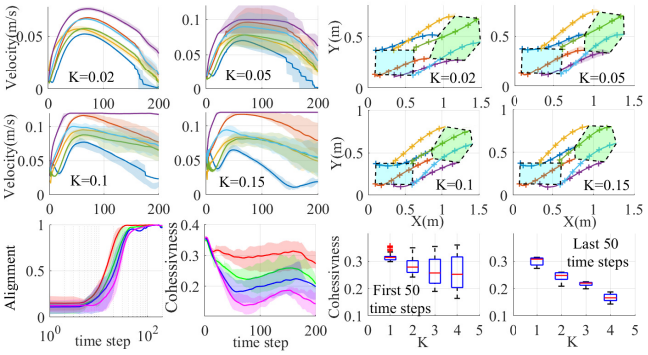

Figure 7. Experiment results for the sensitivity analysis on the stiffness coefficient. (top-left) robots' velocity over time, (top-right) robots' trajectory over time where each colour demonstrates one agent velocity or trajectory in the first two rows, (bottom-left) swarm alignment and cohesiveness over time where the colours are associated to different values for the stiffness as red: $K = 0.02$, green: $K = 0.05$, blue: $K = 0.1$, magenta: $K = 0.15$, (bottom-right) box plot for the cohesiveness in the first and last 50 time steps.

B. Experimental Arena Configuration

To evaluate the applicability of the proposed collective motion model, a series of experiments were conducted involving six robots within a 2×1 m^2 arena. In each experimental trial, the robots were positioned at predefined locations with random orientations, ensuring that each trial starts from a disordered state. A high-resolution camera was installed two meters above the arena and connected to a master PC for comprehensive monitoring of the robot swarm. The robots' movements were accurately tracked using the WhyCon vision-based localisation system [66], which utilises a low-cost webcam to deliver precise position estimates. Each robot was equipped with a unique fiducial circular tag affixed to its top, allowing the WhyCon system to identify and distinguish each robot's position, heading, and ID throughout the experiment.

C. Sensitivity Analysis

According to the analytical development results, three main parameters that play key roles in the algorithm's performance are the stiffness coefficient, the number of neighbours, and the number of scouts, which determine the shape of the Laplacian matrix for the swarm. Therefore, a set of experiments was conducted to evaluate the algorithm's performance considering different conditions for those parameters. In the first set of experiments, the swarm consisted of six robots, one scout, and two neighbours for each robot. The stiffness coefficient was selected from $k \in \{0.02, 0.05, 0.1, 0.15\}$. For each stiffness value, 10 experiments were conducted to evaluate the swarm's behaviour. Fig. 6 shows three frames of the video taken from one of the experiments to visualise the outcomes of the experiment. The results obtained from that set of experiments are presented in Fig. 7.

The results demonstrated in Fig. 7 show the trajectory of the robots and also the velocity variation through time. It is evident from the velocity result that increasing the stiffness coefficient causes the robots to move faster, while also increasing the variation bounds, which results in more uncertainty in the velocity output. On the other hand, the resultant trajectory shows that the final formation geometry depicts larger shifts with respect to the targeted hexagonal shape when the stiffness coefficient is low. Studying the alignment results through time demonstrates a more stable response and convergence for lower stiffness values. However, as discussed in the simulation results, the cohesiveness decreases to lower values when the stiffness parameter is increased. That conclusion is validated by the results obtained from this set of experiments. It is evident from the plots for the cohesiveness in Fig. 7, that increasing the stiffness coefficient decreases the cohesiveness values significantly. According to the box plot, the average value of the cohesiveness in the last 50 time steps of the experiment has been reduced almost linearly by increasing the stiffness coefficient.

The second set of experiments has been conducted to evaluate the effect of the number of neighbours. In that set of experiments, the stiffness coefficient is set as $k = 0.05$, and one scout is considered for the swarm coordination toward the target destination. For a swarm of six robots, two conditions

IEEE Transactions on Automation Science and Engineering (T-ASE) paper, presented at ICRA 2026, Vienna, Austria.

have been considered. In the first set, three neighbours, and in the second set, five neighbours are considered for each robot. For each case, 10 different experiments have been conducted for behavioural analysis. The results obtained from those experiments are demonstrated in Fig. 8. According to the trajectory plot, it is evident that increasing the number of neighbours improved the final formation geometry significantly. Comparing the velocity results in Fig. 8 with the result depicted in Fig. 7 for $k = 0.05$ shows that increasing the number of neighbours reduces the velocity variation bound significantly. However, increasing the number of neighbours from 3 to 5 does not significantly affect the alignment convergence. The cohesiveness index slightly increases as the number of neighbours increases.

In the third set of experiments, the effect of the number of scouts is investigated. In those experiments, the stiffness coefficient was set as $k = 0.05$, and each robot had two neighbours. Two cases were considered to have two and three scouts in the group. Similarly, as in previous studies, 10 experiments were conducted for each case. The results

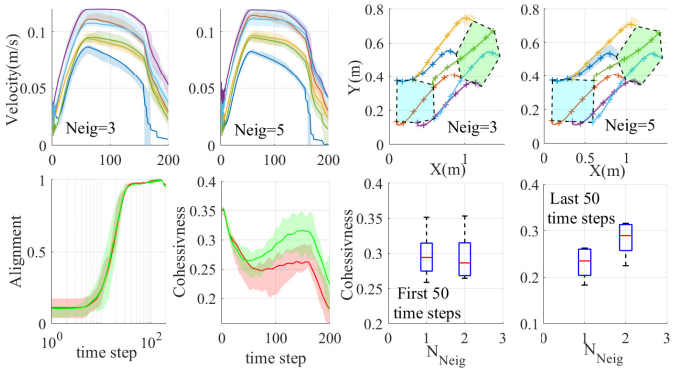

Figure 8. Experiment results for the sensitivity analysis on the number of neighbours. (top-left) robots' velocity over time, (top-right) robots' trajectory over time, (bottom-left) swarm alignment and cohesiveness over time where red lines demonstrate $N_{Neb} = 3$ and green lines demonstrate $N_{Neb} = 5$, (bottom-right) box plot for the cohesiveness in the first and last 50 time steps.

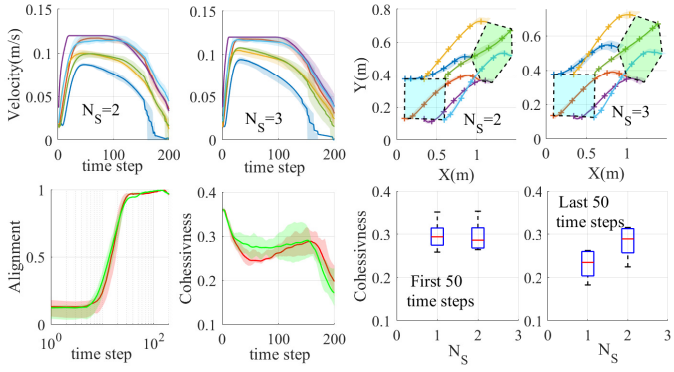

Figure 9. Experiment results for the sensitivity analysis on the number of scouts. (top-left) robots' velocity over time, (top-right) robots' trajectory over time, (bottom-left) swarm alignment and cohesiveness over time, where the red lines demonstrate the $N_S = 2$ and the green lines demonstrate the $N_S = 3$, and (bottom-right) box plot for the cohesiveness in the first and last 50 time steps.

obtained from those experiments are presented in Fig. 9. It is evident from the trajectory plot in Fig. 9 that the final formation geometry is improved by increasing the number of scouts compared to the case presented in Fig. 7 for $k = 0.05$. Although increasing the number of scouts pushes the robots to move faster according to the velocity results in Fig. 9 compared to the velocity plot in Fig. 7, the variation bound is reduced, which demonstrates an improvement in the robustness when we increase the number of scouts.

Although the simulation and experimental results showcase the effectiveness and promising performance of the proposed algorithm, it is necessary to compare the algorithm's performance with that of a state-of-the-art method. Therefore, a set of similar experiments was conducted based on the OCM algorithm with optimised coefficients as presented in [31]. The comparison results are presented in Fig. 10.

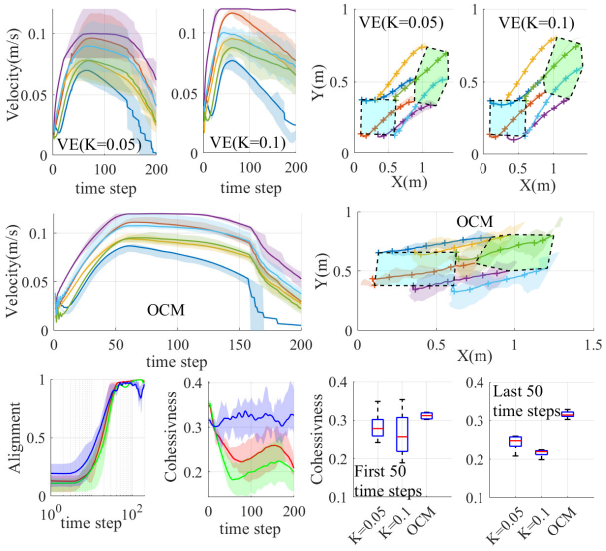

Figure 10. Experiment results for the comparisons between the VE algorithm and the OCM algorithm. (top-left) robots' velocity over time, (top-right) robots' trajectory over time, (bottom-left) swarm alignment and cohesiveness over time, where the red lines demonstrate $VE(K = 0.05)$, the green lines show $VE(K = 0.1)$, and the blue lines show the OCM algorithm's performance. The (bottom-right) box plot is for cohesiveness in the first and last 50 steps.

According to the structure of the OCM method, which is similar to the proposed viscoelastic swarm control in this paper, the outputs exhibit identical behaviours, particularly in terms of the alignment index. However, it is evident that the OCM shows more sensitivity to the uncertainties in the experiments, particularly when the robots reach the steady state condition for alignment. On the other hand, the proposed algorithm demonstrates better performance according to the cohesiveness index, as no considerable change is evident in the OCM results for that index. Furthermore, the trajectory plot illustrates how the proposed algorithm outperforms the OCM method, enabling the robots to achieve the final formation robustly. Nevertheless, the velocity output of both algorithms is quite similar, while the variation bound in the OCM result is smaller than the results obtained from the

IEEE Transactions on Automation Science and Engineering (T-ASE) paper, presented at ICRA 2026, Vienna, Austria.

Table III
COMPARISON OF THE TOTAL FORCE IN THE FIRST 200 TIME STEPS IN THE EXPERIMENTS FOR THE PROPOSED ALGORITHM WITH $k = 0.05, k = 0.1$ AND THE EQUIVALENT FORCE IN THE OCM METHOD.

Algorithm	min	max	median	IQR
VE-k-0.05	0.0025	0.11	0.005	0.0039
VE-k-0.1	0.0036	0.19	0.01	0.0057
OCM	0.0596	0.15	0.076	0.02

proposed algorithm. The primary reason for this difference is related to the nature of the commands in both algorithms. In the OCM method, the velocity command is considered to drive the swarm for alignment and reaching the target points; however, the proposed algorithm incorporates the acceleration command, which causes some fluctuation in the velocity but better results for the final trajectories followed by the robots. In addition to the behavioural comparison, Table III shows an analogy between the total force obtained in three experiments to compare the control effort in the proposed algorithm and the OCM algorithm. As presented in Table III, although the behaviour of the proposed algorithm and the OCM method are similar, the control effort is lower than the OCM method. Although the maximum value obtained for the proposed algorithm with $k = 0.1$ is higher than the total force obtained for the OCM algorithm, the median and IQR indices are much lower than the values obtained for OCM. Therefore, using the proposed algorithm significantly reduces the control effort, which is a key element for algorithms that operate on small robots with substantially limited energy resources.

VI. CONCLUSION

This paper proposes a novel swarm control method that incorporates virtual viscoelastic links between robots in a heterogeneous swarm. The theoretical development demonstrates stability and robustness, considering an arbitrary interaction graph between the agents and bounded disturbances. Furthermore, the theoretical results demonstrate an efficient process for obtaining the algorithm's parameters to satisfy the stability criteria based on the interaction graph. Additionally, twelve sets of Monte Carlo simulations have been conducted for the sensitivity analysis and robust performance evaluation in the presence of measurement noise. According to the sensitivity analysis, it is evident that the stiffness coefficient significantly affects the swarm behaviour, and increasing this variable causes fluctuations in the alignment. However, increasing the stiffness improves the formation rigidity and makes a more cohesive swarm. The same analogy to the number of neighbours and the number of scouts shows improvement in the alignment by increasing the number of neighbours and the number of scouts. The practical capability and robustness of the algorithm were also assessed through a set of experiments that considered multiple cases regarding the key parameters. The performance evaluation demonstrates the algorithm's robustness to the uncertainties in the experiments and validates the theoretical results and simulation. Furthermore, a set of experiments was conducted to compare the algorithm's performance with the state-of-the-art OCM method applying optimised coefficients. Although the behavioural comparison demonstrates similarity in the performance indices, the statistical analysis shows that the proposed algorithm imposes significantly lower control effort on the swarm compared to the OCM method, which is a key element that represents energy consumption and is critical, particularly for small robots. Although the proposed swarm control algorithm guarantees stability and robustness for a swarm of robots with a fixed interaction graph, the swarm control framework for a flexible and time-variant network will be studied in future work to address more practical swarm applications.

Fatemeh Rekabi-Bana received her BSc (2010) and M.Sc. (2012) in Aerospace Engineering from Amirkabir University of Technology (Tehran Polytechnic). She received her PhD (2020) in Mechanical Engineering Dynamics, Control and Vibration from the University of Tehran. She joined the EU-H2020 project (RoboRoyale) as a postdoctoral research associate at the University of Manchester and then at Durham University. She is now working as an Assistant Professor in the Computer Science department at Durham University.

Mazen Bahaidarah received his B.Sc. degree in Computer Engineering from King Abdulaziz University, Jeddah, Saudi Arabia, in 2011, and the M.Sc. degree in Embedded Systems Engineering from the University of Leeds, U.K., in 2018. He is currently a Ph.D. candidate in Electrical Engineering at the University of Manchester, U.K. He began his career as an embedded systems researcher at King Abdulaziz City for Science and Technology (KACST), Riyadh, Saudi Arabia, in 2012. Since 2015, he has been a lecturer at King Abdulaziz University. His research interests include swarm robotics, optimisation algorithms, and embedded systems.

Ognjen Marjanovic (Senior Member, IEEE) received the B.Eng. (Hons.) from the Department of Electrical and Electronic Engineering, Victoria University of Manchester, Manchester, U.K., in 1998, and the Ph.D. degree from the School of Engineering, Victoria University of Manchester, in 2002. He is currently a Reader (Associate Professor) in the Department of Electrical and Electronic Engineering at The University of Manchester, Manchester. His primary research interests include the application of advanced control theory and concepts to address operational challenges in complex real-world systems and processes.

Farshad Arvin (Senior Member, IEEE) received his B.Sc. in Computer Engineering in 2004, his M.Sc. in Computer Systems Engineering in 2010, and his Ph.D. in Computer Science in 2015. He is currently Professor of Robotics in the Department of Computer Science at Durham University, U.K. Before joining Durham, he was Senior Lecturer in Robotics at the University of Manchester. He has held visiting research positions at leading institutes, including the Artificial Life Laboratory at the University of Graz, the Institute of Microelectronics at Tsinghua University, Beijing, and the Italian Institute of Technology (IIT), Genoa. He is the founding director of the Swarm and Computational Intelligence Laboratory (SwaCIL, www.swacil.com), established in 2018. His research focuses on swarm robotics, multi-agent systems, and biohybrid robotics. www.SwaCIL.com.

IEEE Transactions on Automation Science and Engineering (T-ASE) paper, presented at ICRA 2026, Vienna, Austria.

REFERENCES

[1] E. C. Ferrer, T. Hardjono, A. Pentland, and M. Dorigo, "Secure and secret cooperation in robot swarms," *Science Robotics*, vol. 6, no. 56, 2021.

[2] M. Dorigo, G. Theraulaz, and V. Trianni, "Swarm robotics: Past, present, and future [point of view]," *Proceedings of the IEEE*, vol. 109, no. 7, pp. 1152–1165, 2021.

[3] R. S. Parpinelli, G. F. Plichoski, R. S. D. Silva, and P. H. Narloch, "A review of techniques for online control of parameters in swarm intelligence and evolutionary computation algorithms," *International Journal of Bio-Inspired Computation*, vol. 13, no. 1, pp. 1–20, 2019.

[4] N. K. Long, K. Sammut, D. Sgarioto, M. Garratt, and H. A. Abbass, "A comprehensive review of shepherding as a bio-inspired swarm-robotics guidance approach," *IEEE Transactions on Emerging Topics in Computational Intelligence*, vol. 4, no. 4, pp. 523–537, 2020.

[5] M. Saleem, G. A. Di Caro, and M. Farooq, "Swarm intelligence based routing protocol for wireless sensor networks: Survey and future directions," *Information Sciences*, vol. 181, no. 20, pp. 4597–4624, 2011.

[6] L. E. Beaver and A. A. Malikopoulos, "An overview on optimal flocking," *Annual Reviews in Control*, vol. 51, pp. 88–99, 2021.

[7] S. Na, Y. Qiu, A. E. Turgut, J. Ulrich, T. Krajník, S. Yue, B. Lennox, and F. Arvin, "Bio-inspired artificial pheromone system for swarm robotics applications," *Adaptive Behavior*, vol. 29, no. 4, pp. 395–415, 2021.

[8] M. Schranz, G. A. Di Caro, T. Schmickl, W. Elmenreich, F. Arvin, A. Şekercioğlu, and M. Sende, "Swarm intelligence and cyber-physical systems: Concepts, challenges and future trends," *Swarm and Evolutionary Computation*, vol. 60, 2021.

[9] P. Shi and B. Yan, "A survey on intelligent control for multiagent systems," *IEEE Transactions on Systems, Man, and Cybernetics: Systems*, vol. 51, no. 1, pp. 161–175, 2020.

[10] N. Guo, X. Zhang, Y. Zou, B. Lenzo, and T. Zhang, "A computationally efficient path-following control strategy of autonomous electric vehicles with yaw motion stabilization," *IEEE Transactions on Transportation Electrification*, vol. 6, no. 2, pp. 728–739, 2020.

[11] F. Berlinger, M. Gauci, and R. Nagpal, "Implicit coordination for 3d underwater collective behaviors in a fish-inspired robot swarm," *Science Robotics*, vol. 6, no. 50, 2021.

[12] X. Wang and J. Lu, "Collective behaviors through social interactions in bird flocks," *IEEE Circuits and Systems Magazine*, vol. 19, no. 3, pp. 6–22, 2019.

[13] H. El-Fiqi, B. Campbell, S. Elsayed, A. Perry, H. K. Singh, R. Hunjet, and H. A. Abbass, "The limits of reactive shepherding approaches for swarm guidance," *IEEE Access*, vol. 8, pp. 214 658–214 671, 2020.

[14] Y. Xie, L. Han, X. Dong, Q. Li, and Z. Ren, "Bio-inspired adaptive formation tracking control for swarm systems with application to uav swarm systems," *Neurocomputing*, vol. 453, pp. 272–285, 2021.

[15] H. Hamann, *Swarm robotics: A formal approach*. Springer Cham, 2018, vol. 221.

[16] E. Ferrante, A. E. Turgut, M. Dorigo, and C. Huepe, "Collective motion dynamics of active solids and active crystals," *New Journal of Physics*, vol. 15, no. 9, 2013.

[17] R. dell'Erba, "Swarm robotics and complex behaviour of continuum material," *Continuum Mechanics and Thermodynamics*, vol. 31, no. 4, pp. 989–1014, 2019.

[18] M. Raoufi, A. E. Turgut, and F. Arvin, "Self-organized collective motion with a simulated real robot swarm," *Towards Autonomous Robotic Systems*, pp. 263–274, 2019.

[19] M. Bahaidarah, F. Rekabi-Bana, O. Marjanovic, and F. Arvin, "Swarm flocking using optimisation for a self-organised collective motion," *Swarm and Evolutionary Computation*, vol. 86, 2024.

[20] Y. Zheng, C. Huepe, and Z. Han, "Experimental capabilities and limitations of a position-based control algorithm for swarm robotics," *Adaptive Behavior*, vol. 30, no. 1, pp. 19–35, 2022.

[21] T. Nhu, P. D. Hung, V. A. Ho, and T. D. Ngo, "Fuzzy-based distributed behavioral control with wall-following strategy for swarm navigation in arbitrary-shaped environments," *IEEE Access*, vol. 9, pp. 139 176–139 185, 2021.

[22] T. T. Mac, L. M. Quan, B. Q. Dat, and T. N. Sy, "A novel hedge algebra formation control for mobile robots," *Robotics and Autonomous Systems*, vol. 172, p. 104607, 2024.

[23] R. Azzam, I. Boiko, and Y. Zweiri, "Swarm cooperative navigation using centralized training and decentralized execution," *Drones*, vol. 7, no. 3, 2023.

[24] G. Dudek and M. Jenkin, *Computational principles of mobile robotics*. Cambridge University Press, 2024.

[25] S. Zhang, J. Liu, H. Zhang, W. Wang, and Z. Zhang, "Tracking control for multi-agent systems with model switching and topological switching: A novel dual-switch-based dynamic event-triggered approach," *IEEE Transactions on Automation Science and Engineering*, 2024.

[26] Y. Zhu, S. Huang, B. Zuo, D. Zhao, and C. Sun, "Multi-task multi-agent reinforcement learning with task-entity transformers and value decomposition training," *IEEE Transactions on Automation Science and Engineering*, 2024.

[27] F. Rekabi-Bana, F. A. Shirazi, and M. J. Sadigh, "Distributed nonlinear h_∞ control algorithm for multi-agent quadrotor formation flying," *ISA Transactions*, vol. 96, pp. 81–94, 2020.

[28] F. Rekabi-Bana, F. A. Shirazi, M. J. Sadigh, and M. Saadat, "Distributed output feedback nonlinear h_∞ formation control algorithm for heterogeneous aerial robotic teams," *Robotics and Autonomous Systems*, vol. 136, 2021.

[29] M. Doostmohammadian, U. A. Khan, M. Pirani, and T. Charalambous, "Consensus-based distributed estimation in the presence of heterogeneous, time-invariant delays," *IEEE Control Systems Letters*, vol. 6, pp. 1598–1603, 2021.

[30] M. Doostmohammadian and T. Charalambous, "Distributed target tracking based on localization with linear time-difference-of-arrival measurements: A delay-tolerant networked estimation approach," *Systems & Control Letters*, vol. 196, p. 106009, 2025.

[31] M. Bahaidarah, O. Marjanovic, F. Rekabi-Bana, and F. Arvin, "An optimised robot swarm flocking with genetic algorithm," in *IEEE International Conference on Mechatronics and Automation (ICMA)*, 2023, pp. 1823–1828.

[32] M. Bahaidarah, F. R. Bana, A. E. Turgut, O. Marjanovic, and F. Arvin, "Optimization of a self-organized collective motion in a robotic swarm," in *Swarm Intelligence*. Springer International Publishing, 2022, pp. 341–349.

[33] A. Yaqoob, N. K. Verma, M. A. Mir, G. G. Tejani, N. H. B. Eisa, H. Mamoun Hussien Osman, and M. A. Shah, "Sga-driven feature selection and random forest classification for enhanced breast cancer diagnosis: A comparative study," *Scientific Reports*, 2025.

[34] H. Duan, M. Huo, and Y. Fan, "From animal collective behaviors to swarm robotic cooperation," *National Science Review*, vol. 10, no. 5, p. nwad040, 2023.

[35] M. Dratnal, L. Danys, and R. Martinek, "Bio-inspired optimization methods for visible light communication: a comprehensive review," *Artificial Intelligence Review*, 2025.

[36] I. Mir, F. Gul, S. Mir, L. Abualigah, R. A. Zitar, A. G. Hussien, E. M. Awwad, and M. Sharaf, "Multi-agent variational approach for robotics: a bio-inspired perspective," *Biomimetics*, 2023.

[37] M. K. Bijli, P. Verma, and A. P. Singh, "A systematic review on the potency of swarm intelligent nanorobots in the medical field," *Swarm and Evolutionary Computation*, 2024.

[38] D. Maldonado, E. Cruz, J. A. Torres, P. J. Cruz, and S. d. P. G. Benitez, "Multi-agent systems: A survey about its components, framework and workflow," *IEEE Access*, 2024.

[39] J. Ulrich, M. Stefanec, F. Rekabi-Bana, L. A. Fedotoff, T. Rouček, B. Y. Gündeğer, M. Saadat, J. Blaha, J. Janota, D. N. Hofstadler *et al.*, "Autonomous tracking of honey bee behaviors over long-term periods with cooperating robots," *Science Robotics*, vol. 9, no. 95, 2024.

[40] L. Xu, S. Almahri, S. Mak, and A. Brintrup, "Multi-agent systems and foundation models enable autonomous supply chains: Opportunities and challenges," *IFAC-PapersOnLine*, 2024.

[41] L. Sun, Y. Yang, Q. Duan, Y. Shi, C. Lyu, Y.-C. Chang, C.-T. Lin, and Y. Shen, "Multi-agent coordination across diverse applications: A survey," *arXiv preprint arXiv:2502.14743*, 2025.

[42] Y. Alqudsi and M. Makaraci, "Exploring advancements and emerging trends in robotic swarm coordination and control of swarm flying robots: A review," *Proceedings of the Institution of Mechanical Engineers, Part C: Journal of Mechanical Engineering Science*, 2025.

[43] R. Lin, S. Kim, and M. Egerstedt, "Heterogeneous collaborative pursuit via coverage control driven by fokker-planck equations," *IEEE Transactions on Robotics*, 2025.

[44] Y. Cui, Y. Chen, D. Yang, Z. Shu, T. Huang, and X. Gong, "Resilient formation tracking of spacecraft swarm against actuation attacks: A distributed lyapunov-based model predictive approach," *IEEE Transactions on Systems, Man, and Cybernetics: Systems*, vol. 53, no. 11, pp. 7053–7065, 2023.

IEEE Transactions on Automation Science and Engineering (T-ASE) paper, presented at ICRA 2026, Vienna, Austria.

[45] D. Yu, J. Li, Z. Wang, and X. Li, "An overview of swarm coordinated control," *IEEE Transactions on Artificial Intelligence*, vol. 5, no. 5, pp. 1918–1938, 2024.

[46] B. Cetinsaya, D. Reiners, and C. Cruz-Neira, "From pid to swarms: A decade of advancements in drone control and path planning-a systematic review (2013–2023)," *Swarm and Evolutionary Computation*, 2024.

[47] L. McGuire, T. Schuler, M. Otte, and D. Sofge, "Viscoelastic fluid-inspired swarm behavior to reduce susceptibility to local minima: The chain siphon algorithm," *IEEE Robotics and Automation Letters*, vol. 7, no. 2, pp. 1000–1007, 2021.

[48] M. Eguchi, M. Nishimura, S. Yoshida, and T. Hiraki, "Robot swarm control based on smoothed particle hydrodynamics for obstacle-unaware navigation," in *2024 IEEE/RSJ International Conference on Intelligent Robots and Systems (IROS)*, 2024.

[49] Y. Bu, Y. Yan, and Y. Yang, "Advancement challenges in uav swarm formation control: A comprehensive review," *Drones*, 2024.

[50] R. Olfati-Saber, J. A. Fax, and R. M. Murray, "Consensus and cooperation in networked multi-agent systems," *Proceedings of the IEEE*, vol. 95, no. 1, pp. 215–233, 2007.

[51] X.-J. Peng, Y. He, H. Li, and S. Tian, "Robust time-varying formation control of one-sided lipschitz nonlinear multiagent system with delays via optimization algorithm," *IEEE Transactions on Cybernetics*, 2025.

[52] Y. Qian, Z. Miao, J. Zhou, and X. Zhu, "On consensus control of uncertain multiagent systems based on two types of interval observers," *IEEE Transactions on Cybernetics*, 2025.

[53] K. Elamvazhuthi, Z. Kakish, A. Shirsat, and S. Berman, "Controllability and stabilization for herding a robotic swarm using a leader: A mean-field approach," *IEEE Transactions on Robotics*, vol. 37, no. 2, pp. 418–432, 2021.

[54] O. Lasabi, A. Swanson, L. Jarvis, A. Aluko, and A. Goudarzi, "Coordinated hybrid approach based on firefly algorithm and particle swarm optimization for distributed secondary control and stability analysis of direct current microgrids," *Sustainability*, 2024.

[55] J. Janila and A. Lenin Fred, "Multi-robot assisted communication service in disaster areas using fractional chameleon swarm algorithm," *Communications in Statistics-Simulation and Computation*, 2025.

[56] S. Jain and L. Vachhani, "Guided swarm self-clustering in safe area," in *2025 IEEE/SICE International Symposium on System Integration (SII)*, 2025.

[57] M. M. Shahzad, Z. Saeed, A. Akhtar, H. Munawar, M. H. Yousaf, N. K. Baloach, and F. Hussain, "A review of swarm robotics in a nutshell," *Drones*, 2023.

[58] L. Chiani, E. Borgonovo, E. Plischke, and M. Tavoni, "Global sensitivity analysis of integrated assessment models with multivariate outputs," *Risk Analysis*, 2025.

[59] R. C. Smith, *Uncertainty quantification: theory, implementation, and applications*. SIAM, 2024.

[60] Z. Li, W. Ren, X. Liu, and L. Xie, "Distributed consensus of linear multi-agent systems with adaptive dynamic protocols," *Automatica*, vol. 49, no. 7, pp. 1986–1995, 2013.

[61] D. Angeli, E. D. Sontag, and Y. Wang, "A characterization of integral input-to-state stability," *IEEE Transactions on Automatic Control*, vol. 45, no. 6, pp. 1082–1097, 2002.

[62] W. Ren and R. Beard, "Consensus seeking in multiagent systems under dynamically changing interaction topologies," *IEEE Transactions on Automatic Control*, 2005.

[63] A. Tahbaz-Salehi and A. Jadbabaie, "A necessary and sufficient condition for consensus over random networks," *IEEE Transactions on Automatic Control*, 2008.

[64] Y. Saad, *Iterative methods for sparse linear systems*. SIAM, 2003.

[65] F. Arvin, J. Espinosa, B. Bird, A. West, S. Watson, and B. Lennox, "Mona: an affordable open-source mobile robot for education and research," *Journal of Intelligent & Robotic Systems*, vol. 94, no. 3, pp. 761–775, 2019.

[66] T. Krajník, M. Nitsche, J. Faigl, P. Vaněk, M. Saska, L. Přeučil, T. Duckett, and M. Mejail, "A practical multirobot localization system," *Journal of Intelligent & Robotic Systems*, vol. 76, pp. 539–562, 2014.